Progress in Organic Coatings 185 (2023) 107910

Contents lists available at ScienceDirect

Progress in Organic Coatings

journal homepage: www.elsevier.com/locate/porgcoat

A Schiff base-coated ammonia polyphosphate for improving thermal and fire-retardant properties of unsaturated polyester

Jianzhong Zhang [a,1], Yang Fang [a,1], Anlin Zhang [a], Youming Yu [a,*], Lina Liu [a], Siqi Huo [b,**], Xuesen Zeng [b], Hong Peng [c], Pingan Song [b,d,**]

[a] College of Chemistry and Materials Engineering, Zhejiang A & F University, Hangzhou 311300, China
[b] Centre for Future Materials, University of Southern Queensland, Springfield, 4300, Australia
[c] School of Chemical Engineering, The University of Queensland, Brisbane, Qld 4072, Australia
[d] School of Agriculture and Environmental Science, University of Southern Queensland, Springfield, 4300, Australia

ARTICLE INFO

Keywords:
Unsaturated polyester resin
Ammonium polyphosphate
Schiff base
Thermal stability
Flame retardancy

ABSTRACT

Despite extensive applications in modern industry, unsaturated polyester resin (UPR) suffers intrinsic flammability, presenting fire threats to both environment and properties. Existing environmentally benign flame retardants, in particular ammonium polyphosphate (APP), often show a limited efficiency in UPR. Herein, a Schiff base-coated ammonium polyphosphate (MAPP) was synthesized using APP, 1,2-bis(2-aminoethoxy)ethane, and terephthalaldehyde (TPA). The results show that MAPP retards the initial decomposition of UPR and promotes its carbonization under heating, imparting enhanced thermal stability. Notably, 17 wt% of MAPP endows UPR with a UL-94 V-0 rating and a limiting oxygen index (LOI) of 28.6 %. MAPP is also effective in inhibiting heat and smoke release during combustion, and 17 wt% of it brings about 39.5 % and 18.0 % reductions in total heat release and total smoke production. Because of improved interfacial compatibility, the final UPR/MAPP displays significantly improved mechanical properties relative to UPR/APP. This work proposes a new functionalization surface modification strategy for creating efficient APP-based flame retardant for UPR, which is expected to be more widely applied in industries.

1. Introduction

As applications upgrade and stricter standards emerge, higher and more comprehensive requirements have been put forwards for the polymer properties. In particular, more and more attention has been paid to the fire safety of polymeric materials due to the frequent occurrence of fire accidents in recent years [1–3]. Thermosetting polymers have found ubiquitous applications in modern industries due to their superior integrated performances [4–6]. Unsaturated polyester resin (UPR) is one of the most important thermosetting resins [7–9], which features excellent mechanical properties, low density, good corrosion resistance, and low cost [10]. Hence, UPR is extensively applied in various industries, *e.g.*, construction, maritime, transportation, and wind energy [11,12]. However, due to the poor carbonization, UPR is highly combustible, and will release a large number of toxic gases and smoke in the burning procedure, which significantly restricts its applications in daily life [13,14]. To meet the requirements of high-performance applications, it is of great significance to address the flammability issue of UPR.

Ammonium polyphosphate (APP) is an environmentally friendly, halogen-free flame retardant, which has been commonly used to flame retardant UPR [15–18]. During combustion, APP decomposes to generate NH_3, water, and phosphate esters. After the dehydration of phosphate esters, many viscous char layers are formed, and NH_3 and water vapor make the char layers expanded. The intumescent char layers serve as protective shields to retard thermal transfer and isolate pyrolysis products, thus improving flame retardancy [19,20]. However, the unmodified APP suffers from a low flame-retardant efficiency and poor compatibility with the UPR matrix, deteriorating mechanical properties of UPR/APP composites and reducing their practical value [21,22].

To enhance the efficiency and dispersion, many efforts have been

* Co-corresponding author at: College of Chemistry and Materials Engineering, Zhejiang A & F University, Hangzhou 311300, China.
** Corresponding authors at: Centre for Future Materials, University of Southern Queensland, Springfield, 4300, Australia.
E-mail addresses: yuyouming@zafu.edu.cn (Y. Yu), siqi.huo@usq.edu.au (S. Huo), pingan.song@usq.edu.au (P. Song).
[1] These authors contributed equally to this work and were listed as co-first authors.

https://doi.org/10.1016/j.porgcoat.2023.107910
Received 27 June 2023; Received in revised form 1 August 2023; Accepted 20 August 2023
Available online 30 August 2023

made on the surface functionalization of APP [23–26]. For instance, Chen et al. [27] reported a core-shell flame retardant (Dia-APP-TPP) using triphenyl phosphate (TPP) as the shell and APP-coated diatomaceous earth as the core. Adding 20 wt% of Dia-APP-TPP enabled the UPR composite to achieve a UL-94 V-0 rating and a LOI of 26.6 %. When the loading level of Dia-APP-TPP reached 30 wt%, the peak heat release rate (PHRR) and THR of the composite decreased to 344.9 kW/m^2 and 118.4 MJ/m^2, respectively. Jiang et al. [28] prepared a UPR-functionalized APP by grinding UPR and APP, and introduced it (34 wt%), dimethyl methyl phosphate (DMMP, 10 wt%), montmorillonite (MMT, 1 wt%) and zinc borate (ZB, 2 wt%) into UPR to fabricate flame-retardant composite. The as-prepare composite passed a V-0 classification in the UL-94 test and its LOI value increased to 31.3 %. These results demonstrate that the surface functionalization of APP contributes to increasing its efficiency. However, to achieve desirable flame-retardant performances, a relatively high content is still needed for these modified APP additives (>20 wt%). Therefore, it remains a huge challenge for creating high-efficiency APP-based flame retardants for the development of fire-safe UPR composites.

In this study, we constructed a high-efficiency flame retardant (MAPP) by *in-situ* functionalizing APP with Schiff base, and applied it to flame retardant UPR. The impacts of APP and MAPP on the thermal properties, fire retardancy, and mechanical properties of UPR composites were comprehensively investigated. The Schiff base layer endows MAPP with higher flame-retardant efficiency than APP, and enhances the compatibility between MAPP and UPR, allowing UPR/MAPP to achieve superior mechanical properties to UPR/APP. This work provides an effective functionalization approach to enhance the practicability of ammonium polyphosphate in unsaturated polyester resin.

2. Experimental

2.1. Materials

Unsaturated polyester resin (UPR, commercial name: 196#) was provided by Xinyang Technology Group Co., Ltd. (China). Methyl ethyl ketone peroxide (MEKP, initiator, commercial name: Aksu V388), and cobalt isooctanoate (accelerator, commercial name: Tianma E4) were bought from Jiangyin Wanqian Chemical Co., Ltd. (China). Polymerized ammonium polyphosphate (APP, n > 1000) was provided by Shian Chemical Co., Ltd. (China). Ethyl acetate (>99 %), 1,2-bis(2-aminoethoxy)ethane (98 %), and terephthalaldehyde (TPA, 98 %) were purchased from Shanghai Aladdin Biochemical Technology Co., Ltd. (China). All reagents were directly used without further purification.

2.2. Preparation of MAPP

6.7 g (0.05 mol) of TPA was dissolved in 200 mL of ethyl acetate in a beaker. 42.7 g of APP was introduced and stirred continuously. Then, 7.55 g (0.05 mol) of 1,2-bis(2-aminoethoxy)ethane dissolved in 50 mL of ethyl acetate was added dropwise into the beaker, and stirred at 65 °C until the solvent was completely evaporated. The crude product was further dried at 60 °C in a vacuum oven for 24 h, and finally a Schiff base-modified APP (MAPP) was obtained with a yield of 89 %.

2.3. Preparation of UPR and its composites

MAPP was directly blended with UPR, and its dosage was 15 or 17 wt %. The additive amount of MEKP as an initiator was 2 wt% (calculated by UPR mass), and that of cobalt isooctanoate as an accelerator was 1 wt % (calculated by UPR mass). Each UPR mixture was vigorously stirred in a 500 mL flask at a speed of 2000 rpm for 10 min. After degassing, the mixture was poured into a specific stainless-steel mold, and cured for 3 h at 70 °C and 2 h at 100 °C, respectively. The obtained UPR composite containing 15 wt% MAPP was abbreviated as UPR/15MAPP (see Table S1), and the rest were named in the same way. The UPR/APP composite was prepared in the above method, but MAPP was replaced with APP.

2.4. Characterization

Fourier transform infrared spectroscopy (FTIR) was conducted on a Nicolet iS50 FTIR spectrometer (Thermo Fisher Scientific, USA) with the testing range of 4000–400 cm^{-1} and scanning frequency of 32 times. Samples were prepared using potassium bromide disc method.

A TG 209 F3 Tarsus instrument (Netzsch, Germany) was applied to conduct thermogravimetric analysis (TGA) under nitrogen and air atmosphere, respectively. About 10 mg of powder sample was heated from 30 to 800 °C at a heating rate of 10 °C/min. X-ray photoelectron spectroscopy (XPS) was recorded using a K-Alpha XPS spectrometer (Thermo Fisher Scientific, USA).

Field emission scanning electron microscope (SEM) was conducted on a SU8010 scanning electron microscope (Hitachi, Japan), coupled with an energy disperse X-ray spectrometer (EDX). The electron acceleration voltage was 3 kV, and the gold film was sprayed on the sample surface before testing.

Limiting oxygen index (LOI) measurement was performed on a JF-3 oxygen index instrument (Nanjing Jiangning, China) based on GB/T2406.2-2009 standard, with the specimen size of 130 mm * 6.5 mm * 3 mm. Vertical burning (UL-94) test was carried out using a 5402H-V vertical burning tester (Suzhou Yangyi Vouch Co., Ltd., China) according to ASTM D3801 standard, and the specimen size was 130 mm * 13 mm * 3 mm. Cone calorimetry (CONE) test was performed on a cone calorimeter (FTT, UK) in accordance with ISO5660 standard under an external flux of 35 kW/m^2, and the sample size was 100 mm * 100 mm * 3 mm. Fire performance index (FPI) and fire growth index (FGI) were calculated using the following formula:

$$\text{Fire performance index (FPI)} = \text{TTI}/\text{PHRR}$$

$$\text{Fire growth index (FGI)} = \text{PHRR}/t_{\text{PHRR}}$$

where TTI is the time to ignition, PHRR is the peak heat release rate, and t_{PHRR} is the time to PHRR.

Tensile and bending tests were carried out on a CMT6000 universal mechanical testing machine (SANS, China) according to GB/T1040.1-2006 and GB/T9341-2008 standards, with the specimen sizes of 75 mm * 10 mm * 2 mm and 80 mm * 10 mm * 4 mm, respectively. The tensile and bending rates were 2 mm/min, and at least five specimens were tested for each group and the average value was reported.

3. Results and discussions

3.1. Synthesis and characterization of MAPP

Fig. 1a illustrates the synthesis route of MAPP. In short, the synthesis process includes two steps: (1) the synthesis of Schiff base intermediate by the condensation of 1,2-bis(2-aminoethoxy)ethane and TPA, and (2) the formation of Schiff base-containing ammonium polyphosphate (MAPP) by the *in-situ* encapsulation of APP with the intermediate.

The chemical structure of MAPP was firstly characterized by XPS technique, with the spectra shown in Fig. 1b–d. The surface element compositions of APP and MAPP obtained from XPS are listed in Table 1. As presented in Fig. 1b, both APP and MAPP exhibit four binding energy peaks, which are P2p (134.6 eV), C1s (284.7 eV), N1s (401.4 eV) and O1s (532.2 eV), respectively, indicating that no additional element is introduced during the *in-situ* encapsulation. From Table 1, the C content on MAPP surface is 58.61 wt%, much higher than 16.04 wt% on APP surface, while the other element contents are all lower. Obviously, the Schiff base intermediate is rich in carbon element, leading to the increased C content on the MAPP surface. As shown in Fig. 1c, there are three binding energy peaks at 284.8, 286.0 and 286.3 eV in the C1s

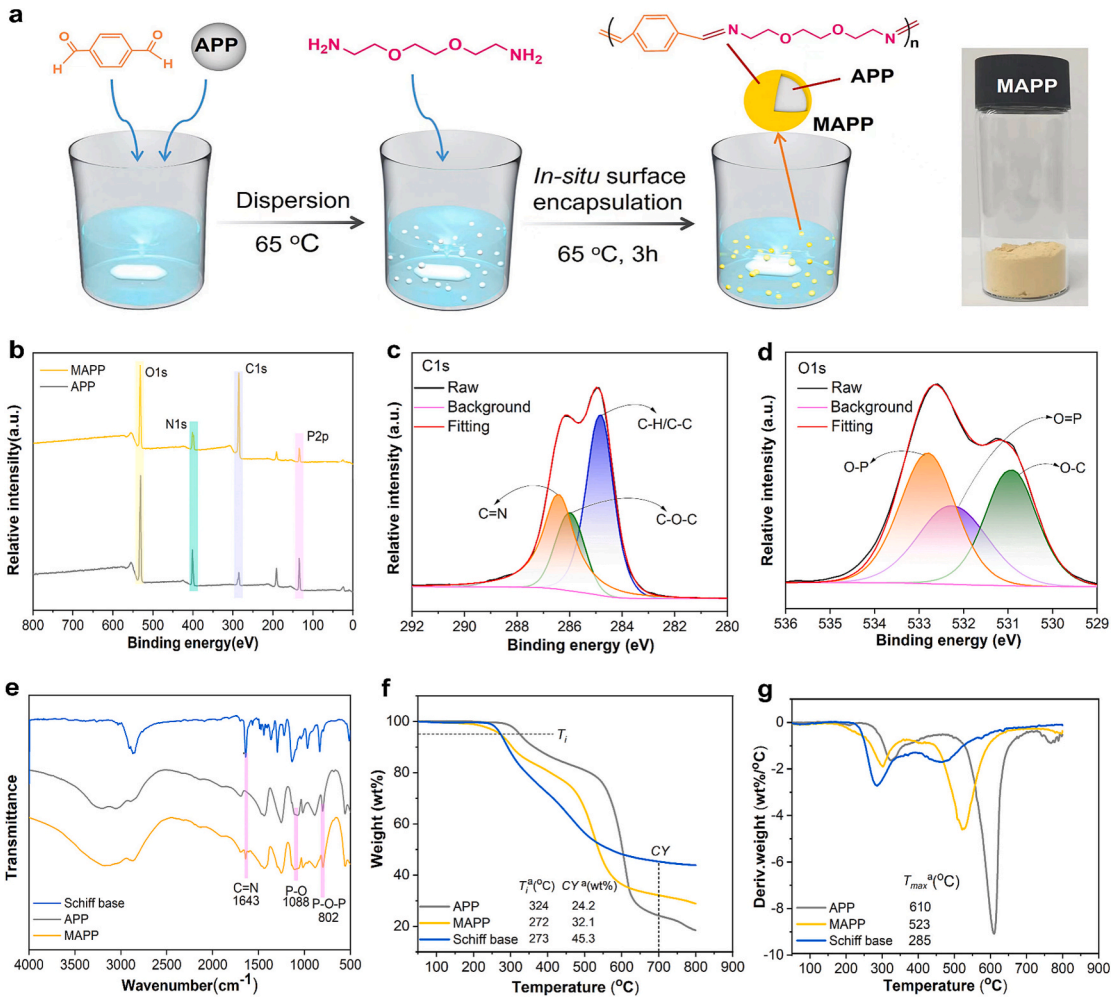

Fig. 1. (a) Synthesis of MAPP, (b) XPS full-scan spectra of MAPP and APP, (c) XPS C1s spectrum of MAPP, (d) XPS O1s spectrum of MAPP, (e) IR spectra of Schiff base intermediate, APP and MAPP, and (f) TG and (g) derivative TG (DTG) curves of Schiff base intermediate, APP, and MAPP in nitrogen condition.

Table 1
The surface elemental contents of APP and MAPP obtained from XPS.

Sample	P (wt%)	N (wt%)	C (wt%)	O (wt%)
APP	17.05	20.36	16.04	46.56
MAPP	5.57	10.71	58.61	25.12

spectrum of MAPP, which are respectively assigned to C—C/C—H, C—O—C and C═N bonds [29,30]. Obviously, the C—O—C bond comes from 1,2-bis(2-aminoethoxy)ethane, and the existence of C═N bond confirms the successful condensation of 1,2-bis(2-aminoethoxy)ethane and TPA on the APP surface. The O1s spectrum of MAPP in Fig. 1d exhibits three binding energy peaks at 531.0, 532.1 and 532.9 eV, which belong to O—C, O═P and O—P structures, respectively. For the P2p spectrum of MAPP in Fig. S1, it shows two binding energy peaks at 133.8 and 134.5 eV, which are corresponded to the P—O and P═O bonds of APP [31]. The XPS results demonstrate that MAPP is successfully synthesized by the *in-situ* encapsulation of APP with Schiff base.

To further confirm the existence of imine bonds in MAPP, the FTIR studies were conducted on Schiff base intermediate, APP, and MAPP. As shown in Fig. 1e, the typical absorption peaks of APP are located at 1088 cm^{-1} (P—O) and 802 cm^{-1} (P—O—P), respectively [19,32]. For MAPP, all typical characteristic peaks derived from APP still exist, but a new absorption peak appears at 1643 cm^{-1}, which is attributed to the stretching vibration of C═N bond [33]. Such results further prove the successful synthesis of MAPP.

The TG and DTG curves of APP, MAPP, and Schiff base intermediate under N_2 atmosphere are shown in Fig. 1f and g. From the TG curves (see Fig. 1f), the initial degradation temperature (temperature at 5 % mass loss, T_i) of APP is as high as 324 °C, while that of MAPP reduces to 272 °C, which is mainly due to the introduction of Schiff base (T_i: 273 °C). Notably, the char yield of APP at 700 °C is 24.2 wt%, while that of MAPP increases to 32.1 wt%, demonstrating that the imine units undergo cross-linking and form chars under elevated temperatures, leading to the improved carbonization ability of MAPP [33]. Similar to T_i, the temperature at maximum mass loss rate (T_{max}) of MAPP reduces from 610 °C of APP to 523 °C. This is probably because the decomposition products of Schiff base promote the degradation of APP at high temperatures [34].

The surface morphologies and element distributions of APP and MAPP were studied by SEM and EDX techniques, with the results shown in Fig. 2 and Table S2. APP exhibits a typical smooth surface (see Fig. 2a). After being modified by Schiff base, the surface morphology of MAPP undergoes significant changes (see Fig. 2b), becoming rough and uneven. Meanwhile, the surface carbon content of MAPP increases relative to that of APP, while the surface nitrogen content decrease (see Fig. 2a_1 and b_1 and Table S2), which is consistent with the XPS result. These results offer compelling evidence for the formation of the Schiff base layer on the surface of MAPP.

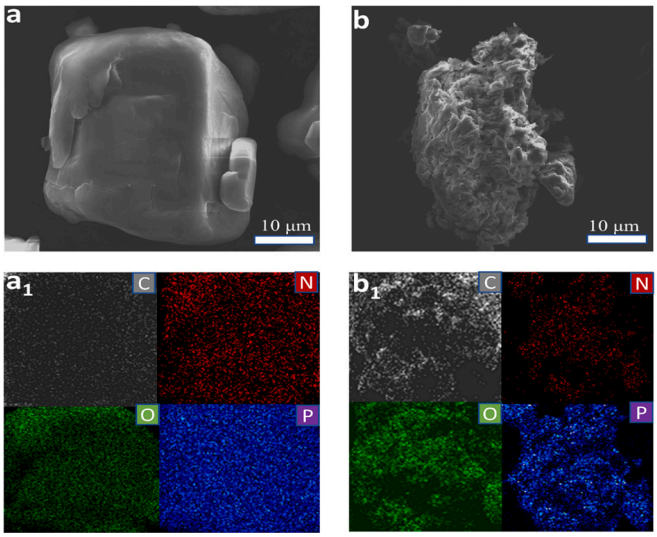

Fig. 2. SEM and element mapping images of (a, a_1) APP and (b, b_1) MAPP.

3.2. Thermal properties of UPR and its composites

The thermal degradation behaviors of UPR and its composites were studied by TGA, with the curves and data presented in Fig. 3 and Table 2. The thermal degradation of all UPR samples under nitrogen atmosphere can be divided into two stages (see Fig. 3a and b). The first stage occurs at 200 to 300 °C, which is mainly caused by the dehydration of the UPR matrix and the decomposition of flame retardants [35]. The second stage at 300–420 °C is the main thermal degradation, which is due to the depolymerization of polystyrene segments and polyester main chains in UPR [36]. Compared with virgin UPR, the maximum weight loss rates of all UPR composites are significantly reduced (see Fig. 3b). In addition, the maximum weight loss rates of UPR/MAPP samples are lower than those of UPR/APP samples, indicating the better promoting carbonization effect of MAPP at high temperatures due to the presence of the Schiff base layer. The promoting carbonization effect of MAPP can also be confirmed by the obviously increased char yields of UPR/MAPP composites as compared to that of UPR. For instance, the char yield of UPR/17MAPP increases from 4.1 wt% of UPR to 26.2 wt%, by about 5-fold. Notably, the introduction of MAPP also brings about the increased T_i of UPR/MAPP. In detail, the T_i of UPR/15MAPP (271 °C) is 36 °C higher than that of UPR (235 °C) in nitrogen condition. In sum, MAPP enhances both thermal stability and char-forming ability of UPR.

Table 2
Thermal performance data of UPR samples under N_2 and air atmosphere.

Sample	T_i (°C)		T_{max} (°C)		Char yield (700 °C, wt%)	
	N_2	Air	N_2	Air	N_2	Air
UPR	235	254	408	408	4.1	0.6
UPR/15APP	254	259	334	335	24.1	14.3
UPR/17APP	270	275	338	339	25.1	16.3
UPR/15MAPP	271	266	336	334	24.9	17.4
UPR/17MAPP	236	265	335	337	26.2	18.6

As shown in Fig. 3c and d, the thermal oxidation decomposition of UPR and its composites consists of three stages. The first stage at 200–310 °C is mainly due to the loss of water in the matrix. The second stage is the major stage (310–410 °C), which is mainly because of the breakdown of the cross-linking network. In this stage, the unstable char layers are formed [37], which decompose at higher temperatures, leading to the appearance of the third decomposition stage. Similarly, the maximum weight loss rates of all UPR composites are lower than that of UPR in air condition, and the char yields are much higher. As shown in Table 2, the char yield of pure UPR is only 0.6 wt% at 700 °C, while that of UPR/17MAPP reaches the highest of 18.6 wt%. This further indicates the superior catalytic effect of MAPP towards the carbonization of the UPR matrix. In addition, the T_i value of UPR under air atmosphere is 254 °C, and those of UPR/15MAPP and UPR/17MAPP increase to 266 and 265 °C, respectively, by 12 and 11 °C. In sum, the introduction of MAPP effectively enhances the thermal stability and carbonization

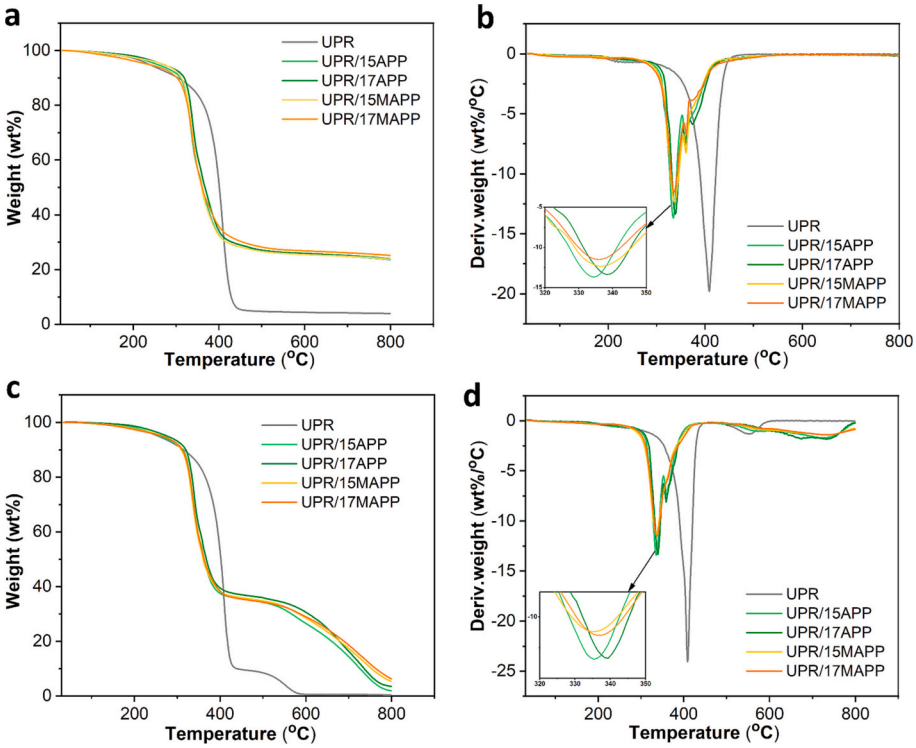

Fig. 3. TG and DTG curves of UPR and its composites under (a, b) nitrogen and (c, d) air atmosphere.

ability of UPR. The superior promoting carbonization effect of MAPP is mainly due to the combined action of Schiff base and APP units [33].

3.3. Flame retardancy of UPR and its composites

To evaluate the flame retardancy of UPR samples, the UL-94 test was first conducted, with the results listed in Table S3. During test, pure UPR sample was easy to be ignited and burned violently to produce a large amount of smoke after ignition, failing to reach any classification. The addition of APP does not significantly improve the flame retardancy of UPR composites, while superior flame retardancy is achieved when replacing APP with MAPP (see Table S3). When the additive amount of MAPP is 15 wt%, the UL-94 rating of UPR/15MAPP reaches V-1. Upon the MAPP content increases to 17 wt%, a UL-94 V-0 rating is obtained. Under the same loading level, MAPP exhibits a higher flame-retardant efficiency than APP, as confirmed by the higher UL-94 ratings of UPR/MAPP than those of UPR/APP. The modification with Schiff base brings about enhanced catalytic carbonization effect of MAPP, enabling it to show higher flame-retardant efficiency towards UPR.

The limiting oxygen index (LOI) is also an important indicator to evaluate the flame retardancy of materials [38]. As shown in Table S3, the LOI of UPR is only 19.6 %, indicating that it is a combustible polymer. The addition of MAPP obviously increases the LOI of UPR. The LOI values of UPR/15MAPP and UPR/17MAPP reach up to 28.2 % and 28.6 %, respectively, indicating that both can be classified into self-extinguishing materials. The UL-94 and LOI results confirm that MAPP can effectively enhance the flame retardancy of UPR by the synergistic effect of Schiff base and APP.

Cone calorimetry (CONE) test can quantitatively evaluate the combustion behaviors of materials by simulating real fire scenarios [39]. The curves and data obtained from CONE tests are shown in Fig. 4 and Table 3. Pure UPR exhibits the shortest time to ignition (TTI) of 43 s, with the highest PHRR (769 kW/m^2) and THR (73.4 MJ/m^2) among all UPR samples (see Table 3), demonstrating that it is easily ignited and release a great deal of heat during burning. With the addition of flame retardants (APP and MAPP), the TTI values of all composites are prolonged, for example, the TTI values of UPR/17APP and UPR/17MAPP are up to 46 and 56 s, respectively. The prolonged TTI allows an increased escape time in a fire. Meanwhile, both MAPP and APP effectively suppressed the heat release of the UPR matrix during combustion (see Fig. 4a and b). Compared with virgin UPR, the PHRR and THR of UPR/17MAPP are reduced by 30.6 % and 39.5 %, respectively, indicative of improved flame retardancy.

As shown in Fig. 4c, due to the poor char-forming ability, pure UPR releases a large amount of toxic smoke in the burning process, of which the TSP and peak smoke production rate (PSPR) reach 22.8 m^2 and 0.231 m^2/s, respectively. Notably, introducing MAPP brings about obviously reduced smoke generation of UPR composites. In particular, UPR/17MAPP displays the lowest TSP and PSPR among all UPR samples, reducing to 18.7 m^2 and 0.206 m^2/s, respectively. Both TSP and PSPR of UPR/17MAPP are lower than those of UPR/17APP, demonstrating that the Schiff base endows MAPP with better smoke suppression function. As displayed in Table 3, the significantly increased residual weight (RW) of UPR/MAPP is responsible for the enhanced smoke suppression. For example, the RW values of UPR/15MAPP and UPR/17MAPP increase to 21.7 and 24.2 wt%, respectively, which are about 6 and 7 times higher than that of UPR control. As mentioned in Section 3.2, the increase in RW of UPR/MAPP is attributed to the catalytic effect of both Schiff base and APP units in MAPP on the formation of char layers [40].

The fire performance index (FPI) and flame propagation index (FGI) are two important parameters for evaluating the fire hazard of materials [41,42]. As shown in Fig. 4e and f, pure UPR exhibits a low FPI of 0.056 FPI m^{2}s/kW and a high FGI of 7.1 kW/m^2/s, demonstrating high fire hazard. With the addition of flame retardants, the FGI decreases and the FPI increases. Among all UPR samples, UPR/15MAPP presents the lowest FGI (2.4 kW/m^2/s) and the highest FPI (0.157 m^{2}s/kW), indicating that the introduction of MAPP imparts superior fire safety to UPR composites.

To further explore the effects of flame retardants on the char

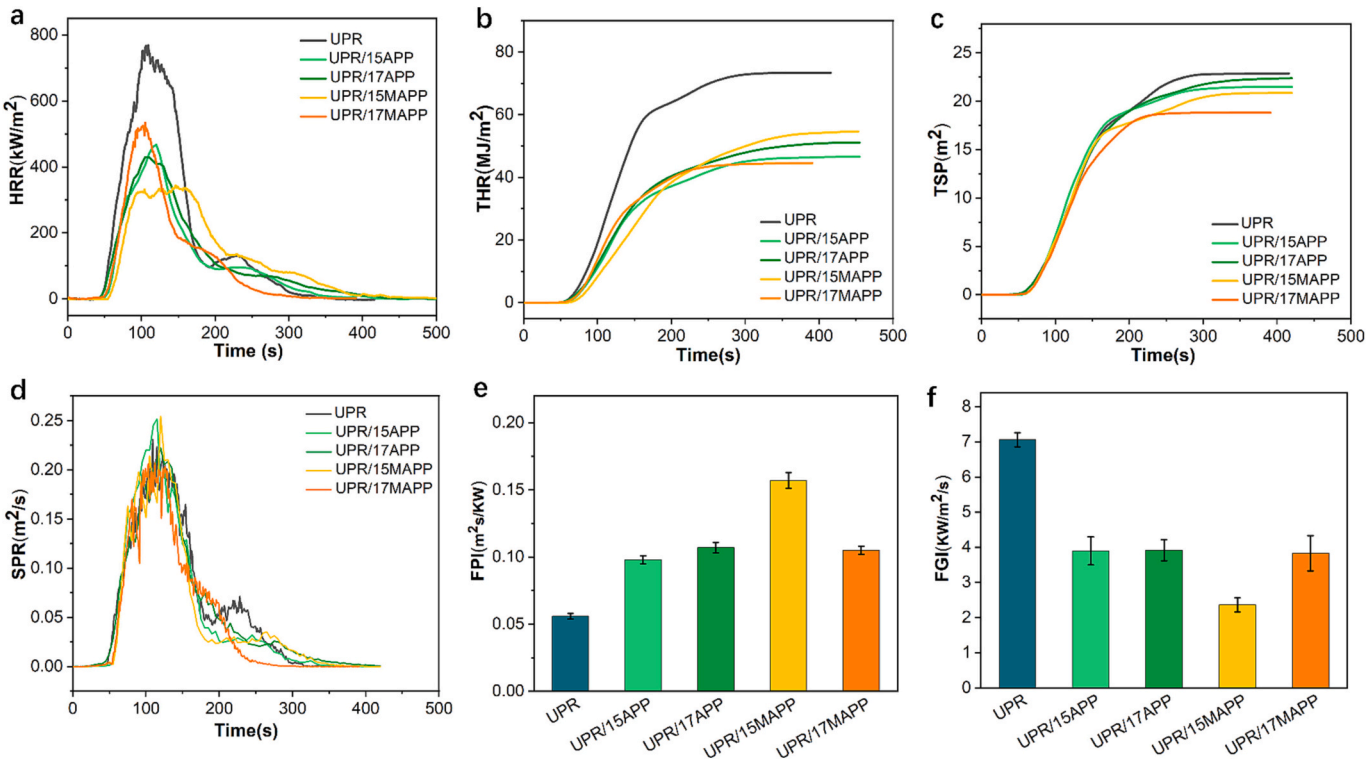

Fig. 4. (a) Heat release rate curves, (b) total heat release plots, (c) total smoke production plots, (d) smoke production rate curves, (e) FPI values, and (f) FGI values of UPR and its composites.

Table 3
Detailed burning data of UPR samples obtained from cone calorimetry tests.

Sample	TTI (s)	PHRR (kW/m^2)	THR (MJ/m^2)	TSP (m^2)	PSPR (m^2/s)	RW (wt%)	FPI (m^{2}s/kW)	FGI (kW/m^2/s)
UPR	43 ± 1	769 ± 15	73.4 ± 2.4	22.8 ± 1.1	0.231 ± 0.012	2.8 ± 0.2	0.056 ± 0.002	7.1 ± 0.2
UPR/15APP	46 ± 2	468 ± 10	46.6 ± 2.3	21.5 ± 1.2	0.252 ± 0.015	20.6 ± 0.3	0.098 ± 0.003	3.9 ± 0.4
UPR/17APP	46 ± 1	430 ± 18	51.1 ± 2.2	22.3 ± 1.3	0.222 ± 0.009	23.3 ± 0.3	0.107 ± 0.004	3.9 ± 0.3
UPR/15MAPP	54 ± 1	344 ± 15	54.8 ± 2.7	20.8 ± 0.9	0.254 ± 0.011	21.7 ± 0.2	0.157 ± 0.006	2.4 ± 0.2
UPR/17MAPP	56 ± 4	534 ± 17	44.4 ± 1.9	18.7 ± 1.4	0.206 ± 0.008	24.2 ± 0.2	0.105 ± 0.003	3.8 ± 0.5

formation, the digital camera and SEM were used, with the photos shown in Fig. 5. UPR almost burns out after CONE test, only leaving few fragile chars (see Fig. 5a). With the introduction of APP and MAPP, the residual chars of UPR composites are greatly increased and their structures become continuous and intumescent. The residual char thicknesses of UPR/15MAPP and UPR/17MAPP reach 3.5 and 4.0 cm, which are higher than those of UPR/15APP (2.0 cm) and UPR/17APP (3.8 cm), further confirming the positive effect of Schiff base on the char formation. In general, an intumescent and continuous char layer can prevent heat/oxygen transfer, inhibit the combustible release, and protect the underlying material from further degradation [43,44]. Therefore, the formation of such intumescent and dense char layers is critical for the improved flame retardancy and smoke suppression of UPR/MAPP.

The microstructure of UPR char is shown in Fig. 5a_2, where abundant irregular pores can be observed on the surface, which is probably caused by tremendous combustible gases breaking through the thin char layers. Notably, the pores on the char surface are significantly reduced after the introduction of APP and MAPP (see Fig. 5c_2 and e_2). In particular, the

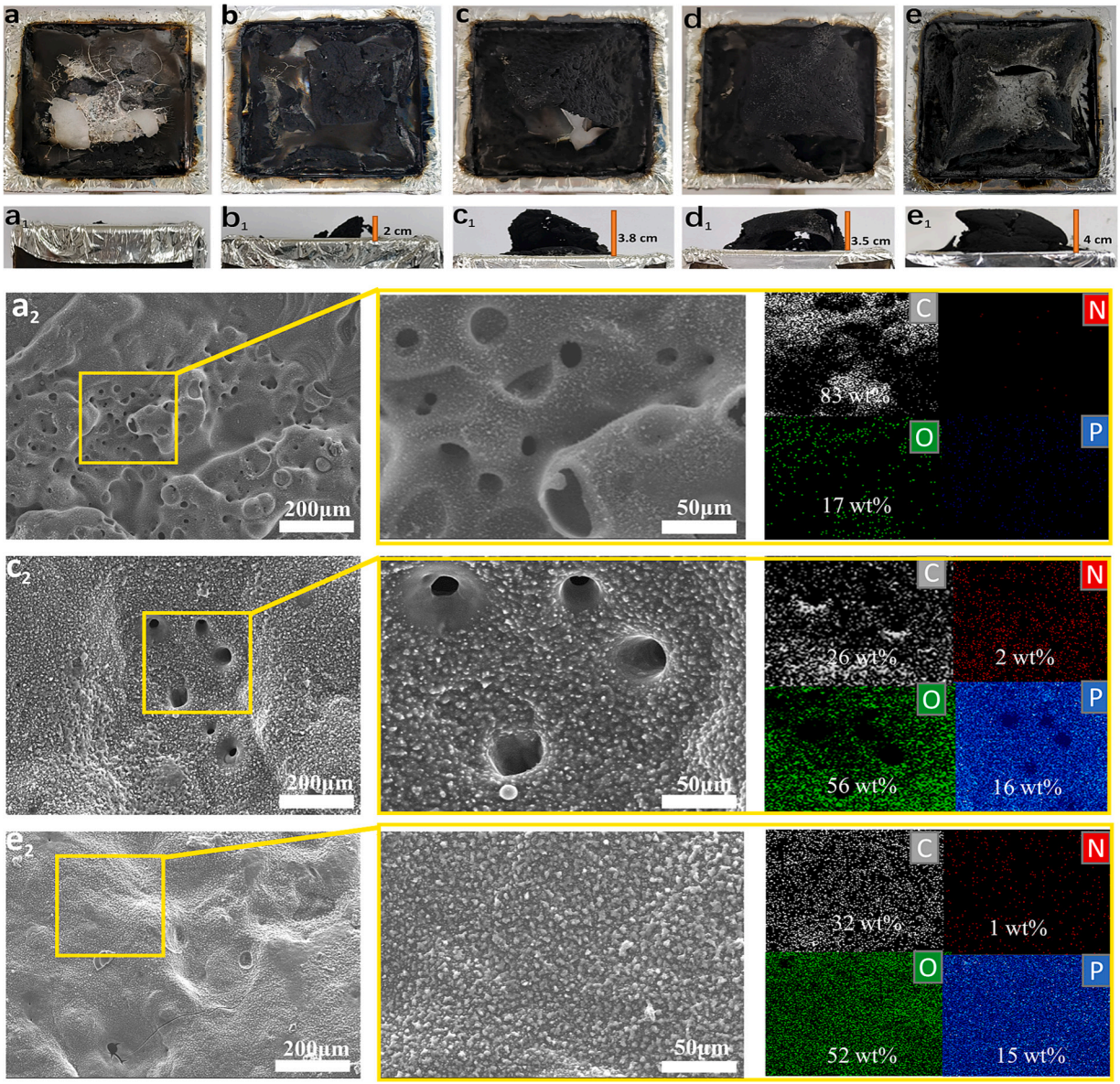

Fig. 5. Digital photos and SEM and elemental mapping images of char residues for UPR and its composites after CONE tests (a: UPR, b: UPR/15APP, c: UPR/17APP, d: UPR/15MAPP, and e: UPR/17MAPP).

pore almost disappears on the surface of UPR/17MAPP char. Meanwhile, the char surface of UPR/17MAPP is continuous and dense, which contributes to suppressing the heat release and smoke generation. The EDX results show that the C content of UPR/17MAPP residue reaches 32 wt%, which is higher than that of UPR/17APP residue (26 wt%), while O, N, and P contents are all lower. Such results further confirm the catalytic effect of Schiff base on the carbonization during burning.

3.4. XPS analysis of residual char

To study the chemical structure and composition of chars, the XPS analyses were conducted on UPR/17APP and UPR/17MAPP residues, with the spectra presented in Figs. 6 and S2. Both XPS full-scan spectra in Fig. S2 display four characteristic binding energy peaks, which are assigned to phosphorus (134.6 eV, P2p), carbon (284.7 eV, C1s), nitrogen (401.4 eV, N1s) and oxygen (532.2 eV, O1s), respectively. The high-resolution C1s and P2p spectra are shown in Fig. 6. Both UPR/17APP and UPR/17MAPP chars display the same deconvoluted peaks in the C1s and P2p spectra, but the C—N and O═P—O—C peak intensities of UPR/17MAPP char are higher than those of UPR/17MAPP char. This is because both Schiff base and APP play catalytic roles in charring, leading to more stable char layers remained in the condensed phase during combustion [33]. Clearly, the catalytic carbonization effect of Schiff base and APP in MAPP is responsible for the enhanced flame retardancy and smoke suppression of UPR/MAPP.

3.5. Mechanical properties of UPR and its composites

The impacts of APP and MAPP on the mechanical properties of UPR were studied by tensile and bending tests, with the results given in Fig. 7 and Table 4. The tensile strength and elastic modulus of pure UPR reach 50.1 MPa and 2.43 GPa, respectively. The introduction of flame retardants reduces the tensile properties of UPR composites. Similar reductions can also be observed in the flexural strengths and moduli of UPR/APP and UPR/MAPP composites. Notably, the mechanical properties of UPR/MAPP are significantly increased in comparison to those of UPR/APP. For instance, under the same loading level of 15 wt%, the tensile strength and elastic modulus of UPR/15APP decrease to 20.2 MPa and 1.23 GPa, while those of UPR/15MAPP reach 36.5 MPa and 2.09 GPa. Additionally, both flexural strength and modulus of UPR/15MAPP are much higher than those of UPR/15APP. Such results indicate that the *in-situ* encapsulation with Schiff base effectively enhances the compatibility between APP and UPR matrix, thus reducing the negative effect of APP on the mechanical properties of UPR [45].

The fractured surface morphologies of UPR and its composites were observed using SEM, with the images presented in Fig. 8. The fractured surface of pure UPR has obvious fluctuations and linear cracks, which is a typical brittle fracture. With the addition of APP, the cross-section of UPR/17APP becomes rough and many APP clusters can be observed (see Fig. 8b). The interface force between APP and matrix is poor, and the existence of APP aggregates tends to cause stress concentration under the external force, thus reducing the mechanical performances of UPR [46,47]. However, the aggregation of MAPP is apparently decreased on the cross-section of UPR/17MAPP (see Fig. 8c), further proving that the presence of the Schiff base layer improves the compatibility between MAPP and UPR, thus endowing UPR/MAPP with improved mechanical properties relative to UPR/APP.

4. Conclusions

In this work, a novel Schiff base-coated APP was successfully synthesized using 1,2-bis(2-aminoethoxy)ethane, TPA and APP as starting materials. The incorporation of MAPP increases both T_i and char yield of UPR/MAPP, demonstrating the improved thermal stability and carbonization ability. UPR/17MAPP with 17 wt% MAPP achieves a UL-94 V-0 rating, with a LOI of 28.6 %. In CONE test, UPR/17MAPP exhibits the lowest THR and TSP values, which decrease by 39.5 % and 18.0 % relative to those of pure UPR, demonstrating superior flame retardancy and smoke suppression. The significantly enhanced fire safety of UPR/MAPP is mainly due to the catalysis of both Schiff base and APP units in MAPP on charring, thus inhibiting the heat release and smoke generation during combustion. In addition, the *in-situ* encapsulation with Schiff base improves the compatibility between APP and UPR, which is conducive to reducing the negative effect of APP on mechanical

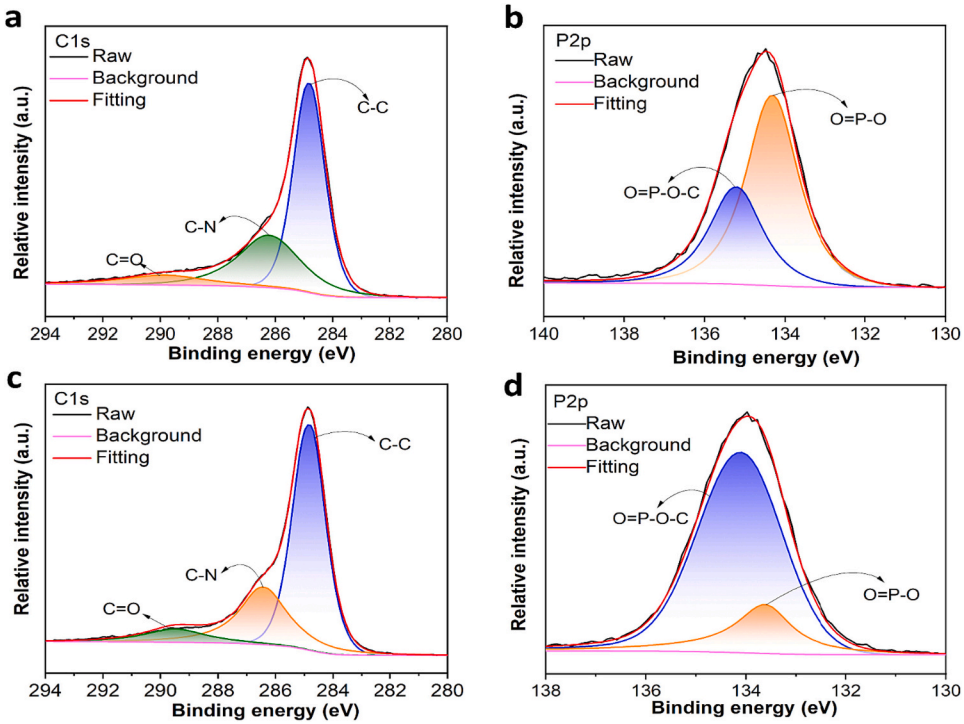

Fig. 6. (a) XPS C1s and (b) P2p spectra of UPR/17APP char, and XPS (c) C1s and (d) P2p spectra of UPR/17MAPP char.

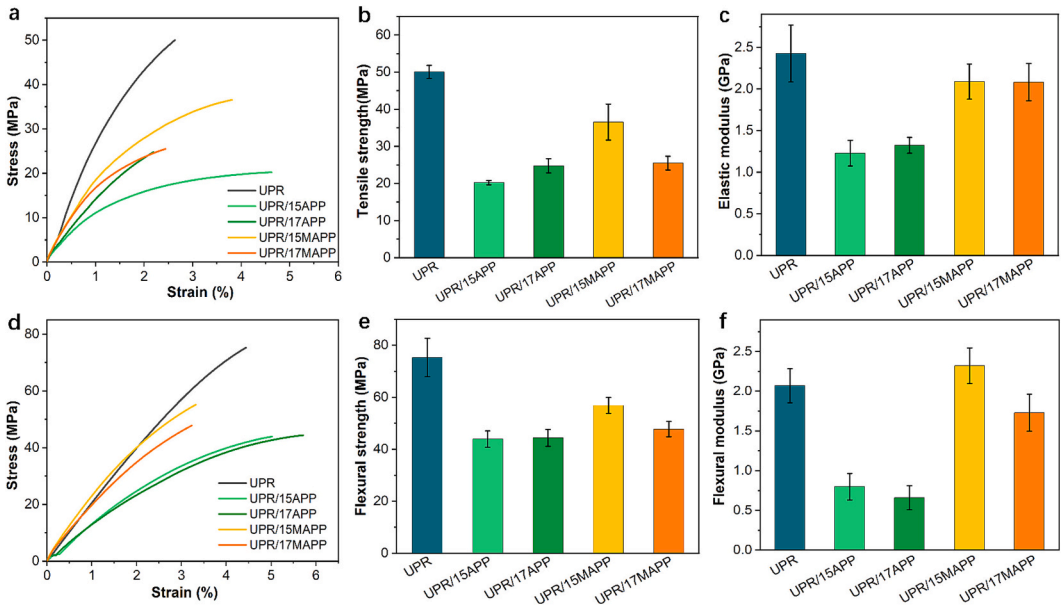

Fig. 7. (a) Tensile stress-strain curves, (b) tensile strengths, (c) elastic moduli, (d) flexural stress-strain curves, (e) flexural strengths, and (f) flexural moduli of UPR samples.

Table 4
Mechanical properties of UPR and its composites.

Sample	Tensile strength (MPa)	Elastic modulus (GPa)	Elongation at break (%)	Flexural strength (MPa)	Flexural modulus (GPa)
UPR	50.1 ± 1.8	2.43 ± 0.30	2.6 ± 0.3	75.3 ± 7.4	2.07 ± 0.22
UPR/15APP	20.2 ± 0.6	1.23 ± 0.15	4.6 ± 0.7	43.9 ± 3.1	0.80 ± 0.17
UPR/17APP	24.8 ± 1.9	1.32 ± 0.10	2.5 ± 0.2	44.4 ± 3.2	0.66 ± 0.15
UPR/15MAPP	36.5 ± 4.8	2.09 ± 0.21	3.8 ± 0.4	56.9 ± 3.0	2.32 ± 0.22
UPR/17MAPP	25.5 ± 1.9	2.08 ± 0.22	2.4 ± 0.3	47.8 ± 2.9	1.73 ± 0.23

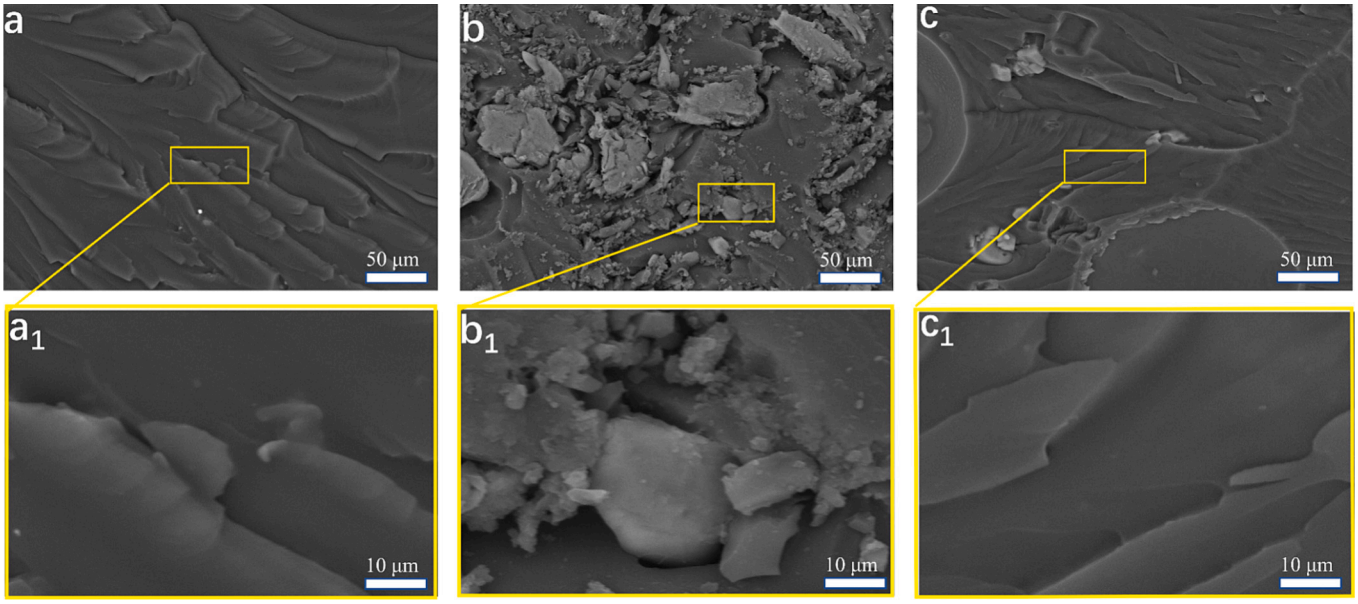

Fig. 8. SEM images of fracture surfaces for (a) UPR, (b) UPR/17APP, and (c) UPR/17MAPP.

properties. This work offers a facile strategy for creating high-efficiency flame retardants for the development of fire-safe UPR composites.

CRediT authorship contribution statement

Jianzhong Zhang: Investigation, Writing – original draft. **Yang Fang:** Investigation, Data curation. **Anlin Zhang:** Formal analysis.

Youming Yu: Formal analysis, Supervision. **Lina Liu:** Data curation. **Siqi Huo:** Supervision, Writing – review & editing. **Xuesen Zeng:** Supervision. **Hong Peng:** Supervision. **Pingan Song:** Project administration, Supervision, Conceptualization, Writing – review & editing.

Declaration of competing interest

The authors declare that they have no known competing financial interests or personal relationships that could have appeared to influence the work reported in this paper.

Data availability

No data was used for the research described in the article.

Acknowledgments

This work was supported by the Australian Research Council (Nos. DP190102992, FT190100188, LP220100278).

Appendix A. Supplementary data

Supplementary data to this article can be found online at https://doi.org/10.1016/j.porgcoat.2023.107910.

References

[1] S. Huo, P. Song, B. Yu, S. Ran, H. Wang, Phosphorus-containing flame retardant epoxy thermosets: recent advances and future perspectives, Prog. Polym. Sci. 114 (2021), 101366.
[2] W. He, P. Song, B. Yu, Z. Fang, H. Wang, Flame retardant polymeric nanocomposites through the combination of nanomaterials and conventional flame retardants, Prog. Mater. Sci. 114 (2020), 100687.
[3] G. Ye, S. Huo, C. Wang, P. Song, Z. Fang, H. Wang, Z. Liu, Durable flame-retardant, strong and tough epoxy resins with well-preserved thermal and optical properties via introducing a bio-based, phosphorus-phosphorus, hyperbranched oligomer, Polym. Degrad. Stabil. 207 (2023), 110235.
[4] Q. Luo, Y. Sun, B. Yu, C. Li, J. Song, D. Tan, J. Zhao, Synthesis of a novel reactive type flame retardant composed of phenophosphazine ring and maleimide for epoxy resin, Polym. Degrad. Stabil. 165 (2019) 137–144.
[5] J. Wang, Y. Liu, X. Guo, H. Qu, J. Ma, Efficient adsorption of dyes using polyethyleneimine-modified NH_2-MIL-101(Al) and its sustainable application as a flame retardant for an epoxy resin, ACS Omega 5 (50) (2020) 32286–32294.
[6] Q. Chen, L. Liu, A. Zhang, W. Wang, Z. Wang, J. Zhang, J. Feng, S. Huo, X. Zeng, P. Song, An iron phenylphosphinate@ graphene oxide nanohybrid enabled flame-retardant, mechanically reinforced, and thermally conductive epoxy nanocomposites, Chem. Eng. J. 454 (2023), 140424.
[7] F.A.M.M. Gonçalves, A.C. Fonseca, M. Domingos, A. Gloria, A.C. Serra, J.F. J. Coelho, The potential of unsaturated polyesters in biomedicine and tissue engineering: synthesis, structure-properties relationships and additive manufacturing, Prog. Polym. Sci. 68 (2017) 1–34.
[8] Y. Lin, B. Yu, X. Jin, L. Song, Y. Hu, Study on thermal degradation and combustion behavior of flame retardant unsaturated polyester resin modified with a reactive phosphorus containing monomer, RSC Adv. 6 (55) (2016) 49633–49642.
[9] Y. Hou, W. Hu, Z. Gui, Y. Hu, Effect of cuprous oxide with different sizes on thermal and combustion behaviors of unsaturated polyester resin, J. Hazard. Mater. 334 (2017) 39–48.
[10] L. Tibiletti, C. Longuet, L. Ferry, P. Coutelen, A. Mas, J.J. Robin, J.M. Lopez-Cuesta, Thermal degradation and fire behaviour of unsaturated polyesters filled with metallic oxides, Polym. Degrad. Stabil. 96 (1) (2011) 67–75.
[11] N.O. Camlibel, Polyester — production, characterization and innovative applications, in: Flame-retardant Unsaturated Polyester Resins: An Overview of Past and Recent Developments, 2018, https://doi.org/10.5772/intechopen.69941 (Chapter 3).
[12] E.D. Weil, S.V. Levchik, Commercial flame retardancy of unsaturated polyester, vinyl resins, phenolics and their composites, in: Flame Retardants for Plastics and Textiles, 2009, pp. 141–152.
[13] J.R. Ebdon, Thermal stability, flammability and mechanical performances of unsaturated polyester–melamine resin blends and of glass fibre-reinforced composites based on them, Polymers 14 (2022) 4885.
[14] D. Wang, Y. Kan, X. Yu, J. Liu, L. Song, Y. Hu, In situ loading ultra-small Cu_2O nanoparticles on 2D hierarchical TiO_2-graphene oxide dual-nanosheets: towards reducing fire hazards of unsaturated polyester resin, J. Hazard. Mater. 320 (2016) 504–512.
[15] A. Hassan, L.Y. Hau, M. Hasan, Effect of ammonium polyphosphate on flame retardancy, thermal stability, and mechanical properties of unsaturated polyester/phenolic/montmorillonite nanocomposites, Adv. Polym. Technol. 36 (2017) 278–283.
[16] J. Reuter, L. Greiner, P. Kukla, M. Dring, Efficient flame retardant interplay of unsaturated polyester resin formulations based on ammonium polyphosphate, Polym. Degrad. Stabil. 178 (2020), 109134.
[17] L.L. Pan, G.Y. Li, Y.C. Su, J.S. Lian, Fire retardant mechanism analysis between ammonium polyphosphate and triphenyl phosphate in unsaturated polyester resin, Polym. Degrad. Stabil. 97 (9) (2012) 1801–1806.
[18] Y. Shih, Y. Wang, R. Jeng, K. Wei, Expandable graphite systems for phosphorus-containing unsaturated polyesters. I. Enhanced thermal properties and flame retardancy, Polym. Degrad. Stabil. 86 (2) (2004) 339–348.
[19] Z.B. Shao, D. Cong, T. Yi, M.J. Chen, L. Chen, Y.Z. Wang, Flame retardation of polypropylene via a novel intumescent flame retardant: ethylenediamine-modified ammonium polyphosphate, Polym. Degrad. Stabil. 106 (2014) 88–96.
[20] Y. Hong, Z. Zhao, Y. Wang, Q. Jin, X. Zhang, Structural modification of ammonium polyphosphate by DOPO to achieve high water resistance and hydrophobicity, Powder Technol. 320 (2017) 14–21.
[21] M. Chen, Y. Xu, X. Chen, Y. Ma, W. He, J. Yu, Z. Zhang, Thermal stability and combustion behavior of flame-retardant polypropylene with thermoplastic polyurethane-microencapsulated ammonium polyphosphate, High Perform. Polym. 26 (2014) 445–454.
[22] Z. Jiang, G. Liu, Microencapsulation of ammonium polyphosphate with melamine-formaldehyde-tris(2-hydroxyethyl)isocyanurate resin and its flame retardancy in polypropylene, RSC Adv. 5 (2015) 88445–88455.
[23] K. Wu, Z. Wang, H. Liang, Microencapsulation of ammonium polyphosphate: preparation, characterization, and its flame retardance in polypropylene, Polym. Compos. 29 (8) (2010) 854–860.
[24] K. Wu, Z. Wang, Y. Hu, Microencapsulated ammonium polyphosphate with urea–melamine–formaldehyde shell: preparation, characterization, and its flame retardance in polypropylene, Polym. Adv. Technol. 19 (2008) 1118–1125.
[25] Jiao, Chen, Zhang, Microencapsulation of ammonium polyphosphate with hydroxyl silicone oil and its flame retardance in thermoplastic polyurethane, J. Therm. Anal. Calorim. 104 (2011) 1037–1043.
[26] N. Mao, L. Jiang, X. Li, Y. Gao, Y. Zhai, Core-shell ammonium polyphosphate@ nanoscopic aluminum hydroxide microcapsules: preparation, characterization, and its flame retardancy performance on wood pulp paper, Adv. Chem. Eng. 6 (2021), 100096.
[27] Z. Chen, M. Jiang, Z. Chen, T. Chen, J. Jiang, Preparation and characterization of a microencapsulated flame retardant and its flame-retardant mechanism in unsaturated polyester resins, Powder Technol. 354 (2019) 71–81.
[28] M. Jiang, Y. Zhang, Y. Yu, Q. Zhang, B. Huang, Z. Chen, T. Chen, J. Jiang, Flame retardancy of unsaturated polyester composites with modified ammonium polyphosphate, montmorillonite, and zinc borate, J. Appl. Polym. Sci. 136 (2019) 47180.
[29] L. Chen, T. Fu, H.B. Zhao, D.M. Guo, X.L. Wang, Y.Z. Wang, New application for aromatic Schiff base: high efficient flame-retardant and anti-dripping action for polyesters, Chem. Eng. J. 336 (2018) 622–632.
[30] X. Dong, L. Chen, R.T. Duan, Y.Z. Wang, Phenylmaleimide-containing PET-based copolyester: cross-linking from $2\pi + \pi$ cycloaddition toward flame retardance and anti-dripping, Polym. Chem. 2698-2708 (2016).
[31] Z. Chen, M. Jiang, Z. Chen, T. Chen, Y. Yu, J. Jiang, Preparation and characterization of a microencapsulated flame retardant and its flame-retardant mechanism in unsaturated polyester resins, Powder Technol. 354 (2019) 71–81.
[32] G. Liu, X. Liu, J. Yu, Ammonium polyphosphate with crystalline form V by ammonium dihydrogen phosphate process, Ind. Eng. Chem. Res. 49 (12) (2010) 5523–5529.
[33] C. Ding, S. Zhang, M. Pan, M.C. Li, C. Mei, Improved processability and high fire safety of wood plastic composites via assembling reversible imine crosslinking network, Chem. Eng. J. 423 (11) (2021), 130295.
[34] S. Zhang, Z. Chen, M. Ding, T. Yang, M. Wang, Reducing the fire toxicity of wood composites using hierarchically porous 4A (H4A) zeolite modified ammonium polyphosphate (APP) synthesized by a facile in-situ method, Constr. Build. Mater. 262 (12) (2020), 120754.
[35] Y. Lin, S. Jiang, Y. Hu, G. Chen, X. Shi, X. Peng, Hybrids of aluminum hypophosphite and ammonium polyphosphate: highly effective flame retardant system for unsaturated polyester resin, Polym. Compos. 39 (2018) 1763–1770.
[36] Z. Bai, S. Lei, H. Yuan, X. Gong, R. Yuen, Investigation on flame retardancy, combustion and pyrolysis behavior of flame retarded unsaturated polyester resin with a star-shaped phosphorus-containing compound, J. Anal. Appl. Pyrol. 105 (2014) 317–326.
[37] E. Kandare, B.K. Kandola, D. Price, S. Nazaré, R.A. Horrocks, Study of the thermal decomposition of flame-retarded unsaturated polyester resins by thermogravimetric analysis and Py-GC/MS, Polym. Degrad. Stabil. 93 (11) (2008) 1996–2006.
[38] Y. Zhang, X. Li, Z. Cao, Z. Fang, T. Richard, Synthesis of zinc phosphonated poly (ethylene imine) and its fire-retardant effect in low-density polyethylene, Ind. Eng. Chem. Res. 54 (13) (2015) 3247–3256.
[39] G. You, Z. Cheng, Y. Tang, H. He, Functional group effect on char formation, flame retardancy and mechanical properties of phosphonate–triazine-based compound as flame retardant in epoxy resin, Ind. Eng. Chem. Res. 54 (30) (2015) 7309–7319.
[40] X. Lu, X. Gu, A sustainable lignin-based epoxy resin: its preparation and combustion behaviors, Ind. Crop. Prod. 192 (2023), 116151.
[41] S.M. Seraji, P. Song, R.J. Varley, S. Bourbigot, D. Voice, H. Wang, Fire-retardant unsaturated polyester thermosets: the state-of-the-art, challenges and opportunities, Chem. Eng. J. 430 (2022), 132785.
[42] Q. Yang, J. Wang, X. Chen, S. Yang, S. Huo, Q. Chen, P. Guo, X. Wang, F. Liu, W. Chen, P. Song, H. Wang, A phosphorus-containing tertiary amine hardener

enabled flame retardant, heat resistant and mechanically strong yet tough epoxy resins, Chem. Eng. J. 468 (2023), 143811.
[43] Y. Yu, S. Jiang, F. Sun, Synthesis and properties of a photopolymerizable carbene-mediated poly phosphinate flame retardant by carbene polymerization, Ind. Eng. Chem. Res. 53 (42) (2014) 16135–16142.
[44] J. Wang, S. Huo, J. Wang, S. Yang, K. Chen, C. Li, D. Fang, Z. Fang, P. Song, H. Wang, Green and facile synthesis of bio-based, flame-retardant, latent imidazole curing agent for single-component epoxy resin, ACS Appl. Polym. Mater. 4 (5) (2022) 3564–3574.
[45] S. Zhang, F. Chu, Z. Xu, Y. Zhou, W. Hu, Y. Hu, Interfacial flame retardant unsaturated polyester composites with simultaneously improved fire safety and mechanical properties, Chem. Eng. J. 426 (2021), 131313.
[46] X. Xu, J. Dai, Z. Ma, L. Liu, P. Song, Manipulating interphase reactions for mechanically robust, flame-retardant and sustainable polylactide biocomposites, Compos. Pt. B Eng. 190 (2020), 107930.
[47] L. Liu, B. Shi, A. Zhang, Y. Xue, J. Zhang, J. Dai, M. Hassanpour, L.C. Tang, Y. Shi, P. Song, A polyphosphoramide-grafted lignin enabled thermostable and fire-retardant polylactide with preserved mechanical properties, Compos. Pt A Appl. Sci. Manuf. 160 (2022), 107028.